NASA

Technical Memorandum 80725

Thermal Structure and Dynamics of the Jovian Atmosphere

I. The Great Red Spot

F. Michael Flasar, Barney J. Conrath, Joseph A. Pirraglia, Patrick C. Clark, Richard G. French and Peter J. Gierasch

NOVEMBER 1980

National Aeronautics and Space Administration

Goddard Space Flight Center
Greenbelt, Maryland 20771

THERMAL STRUCTURE AND DYNAMICS OF THE JOVIAN ATMOSPHERE
I. THE GREAT RED SPOT

F. MICHAEL FLASAR
BARNEY J. CONRATH
JOSEPH A. PIRRAGLIA
NASA/Goddard Space Flight Center
Greenbelt, Maryland 20771

PATRICK C. CLARK
RICHARD G. FRENCH
AND
PETER J. GIERASCH
Cornell University
Ithaca, NY 14853

June 1980
REVISED NOVEMBER 1980

ABSTRACT

Temperatures and thermal winds, derived from Voyager IRIS data over the Great Red Spot and its environs, are presented. The atmosphere over the GRS is characterized by a tropopause which is cold relative to its environment and an upper stratosphere which is relatively warm. The cold tropopause implies a decrease in anticyclonic vorticity with height above 500 mb through the lower stratosphere. IRIS observations at 5μm indicate little emission from the GRS itself, but enhanced emission in a ring about it, in agreement with recent ground-based results. The behavior of the tropopause and 5μm temperatures can be consistently interpreted as resulting from a circulation which rises within the GRS and subsides in the area around it. The explanation of the upper stratospheric temperatures is not so straightforward. A previous suggestion that they may be a manifestation of the linear vertical propagation of Rossby waves appears inconsistent with the gross east-west symmetry in the stratospheric temperatures over the GRS. The implications of the present results for various theoretical models of the GRS are examined, and the possibility that latent heat release drives the GRS is discussed. Dynamical scalings based on an axisymmetric, frictionally controlled vortex suggest that, aside from the nonlinearities inherent in the parameterization of small-scale moist convection, the large-scale dynamics of the GRS are linear, as distinct from those of a tropical cyclone, which are markedly nonlinear.

Introduction

One of the objectives of the Voyager infrared spectroscopy investigation (IRIS) is the study of the thermal structure and dynamics of the Jovian atmosphere, on both global and local scales. One of the more interesting features studied has been the Great Red Spot, which has been continually observed for the past 100 years and probably has existed 300 years or longer (Peek, 1958). In a preliminary report, Hanel et al. (1979a) pointed out the existence of relatively low temperatures in the upper troposphere and lower stratosphere above the GRS. Orton (1975) had tentatively reached a similar conclusion based on analysis of Pioneer 10 broad-band radiometer data. However, the IRIS data have sufficiently high horizontal spatial resolution that, for the first time, the detailed thermal structure associated with the GRS can be studied.

In this paper we first present the temperature fields associated with the GRS, derived from the IRIS data for atmospheric pressures $500 > p(mb) > 3$. We discuss the tangential winds implied by these temperatures from the thermal wind relation. We summarize the structure observed at 5 μm. We then examine the dynamics implied by the observed thermal structure. Finally, we discuss our results in the context of several theoretical models of the GRS. Latent heat release as an energy source for the GRS is considered, and the analogies with and differences from tropical cyclones on Earth are discussed.

Observations and Results

Approximately 18 hours before the closest approach to Jupiter of the Voyager 1 flyby, spectra were obtained in orthogonal scans nearly aligned with the (east-west) major and (north-south) minor axes of the GRS. The resulting "cross" extended into the regions adjacent to the spot and is depicted in Figure 1. Two spectra were acquired at each point of observation and averaged. Vertical temperature profiles over the range 500 mb to 3 mb were then derived by using measured radiances at selected frequencies as discussed by Conrath and Gautier (1980). Temperatures in the upper troposphere ($100 < p\ (mb) < 500$) were obtained by selecting

frequencies within the S(0) and S(1) hydrogen absorption lines. Since these lines are quite broad, the radiances were not taken directly from the original pair-average spectra. Instead, to improve the signal-to-noise ratio, they were taken from second-order polynomials fit to the spectra in a least-square sense over a 20 to 40 cm^{-1} interval at each selected frequency. An exception was the radiance at 285 cm^{-1}, because of the contribution of NH_3 at nearby wavenumbers; in any case, the noise level of brightness temperature in this region of the spectrum is quite low. The resulting formal error of the temperatures so retrieved is < 1 K with an effective vertical resolution of 1/2 to 1 scale height. Temperatures in the upper stratosphere (3 < p (mb) < 10) were obtained from data at 1304.3 cm^{-1} within the CH_4 band, where the signal-to-noise ratio is lower, and the formal error in the retrieved temperatures may exceed 5 K. The effective vertical resolution here is approximately 2 scale heights. Temperature information in the range 10 < p (mb) < 100 was provided only by the low-pressure wing of the CH_4 weighting function corresponding to 1304.3 cm^{-1} and the high-pressure wing of the hydrogen weighting function corresponding to 602 cm^{-1}. Radiances at 1297.3 cm^{-1} and 1301.1 cm^{-1} were not used in the temperature inversions because of their low signal-to-noise ratio. Consequently the detailed vertical structure of this part of the stratosphere is poorly known.

East-west and north-south vertical cross sections of the temperature fields in the vicinity of the GRS are presented in Figure 2. Preliminary cross sections were given by Hanel et al. (1979a). In Fig. 2 the temperatures indicated are deviations (K) from the average of the temperature profiles obtained from the cross sequence. At the time of these measurements, the visible spot was centered at 23°S, 77°W. The atmosphere over the spot is relatively cold in the upper troposphere and lower stratosphere (the tropopause level is located at approximately 100 mb). In the east-west cross section, the upper stratosphere is relatively warm over the spot. Moreover, the stratospheric temperatures are, in a gross sense, symmetric about the central longitude of the spot. This symmetry has important implications for the source of the thermal structure in the stratosphere, as will be discussed shortly. The stratospheric temperatures

above 10 mb in the north-south cross section are quite asymmetric about the central latitude of the spot and may reflect the imbedding of the spot in Jupiter's zone-belt system.

The temperature fields can also furnish useful information about the winds associated with the GRS. If the tangential velocities are in geostrophic balance, and the vertical variation in pressure (including those components associated with motions) is governed by hydrostatic balance, then the tangential velocity, u, obeys the thermal wind equation (cf. Holton, 1972)

$$\left(\frac{\partial u}{\partial \ln p}\right)_r = - \frac{R}{f} \left(\frac{\partial T}{\partial r}\right)_p \quad ; \qquad (1)$$

u is defined to be positive for counterclockwise flow, f is the Coriolis parameter, negative in the southern hemisphere, R is the gas constant of the Jovian atmosphere, p is pressure, T is temperature, and r is a coordinate vector directed normal to the tangential velocity and outward. Along the major and minor axes of the GRS, r is equivalently the radial distance from its center. The assumption of geostrophic balance requires that the Rossby number (Ro = characteristic tangential velocity/(f x horizontal scale of GRS)) be small. Smith et al. (1979a) estimate it to be of $O(10^{-1})$ at the visible cloud top level. The assumption of hydrostatic balance requires that the vertical dimension/horizontal dimension of the GRS circulation be small. As discussed later, vertical scales $\sim 10\text{-}10^2$ km are not unreasonable, yielding a ratio $\leq 10^{-2}$. Eq. (1) also assumes that frictional forces can be neglected. About friction we can say nothing a priori.

We have integrated (1), using the derived temperature fields, to obtain tangential winds as a function of pressure. In doing this we have arbitrarily specified that u be zero at a pressure of 22 mb. The resulting wind fields are presented in Figure 3. The formal uncertainty in the 500 mb thermal winds is 10-15 m s^{-1}, except on the northern portion of the cross, where smaller values of f result in larger errors. In Figure 3 there is a well defined anticyclonic vortex in the lower stratosphere and upper troposphere. The structure is resolved better in the east-west vertical

cross section, which indicates that the velocity field near the center of the spot is not well organized. The vortex is annular, with the angular velocity, u/r, largest well away from the center of the spot. The annular region is quite thick and extends outward well beyond the visible spot (c.f. Figs. 1 and 3). Even allowing for the IRIS field of view, a thickness of $6\text{-}9^{\circ}$ in longitude is indicated.

Mitchell *et al.* (1981), from velocity measurements of visible clouds within the GRS, have also found that the flow field exhibits an annular structure. Along the major axis maximum velocities occur 9° in longitude from the center of the spot; this corresponds to the inner portion of the thermal wind vortex in Fig. 3a. Measured velocities of visible clouds at greater distances were not available. The maximum cloud velocities measured have a mean value of 110 m s^{-1}, although the dispersion about this mean is large. Mitchell *et al.* have argued that this mean is representative of the flow field all around the spot. The maximum thermal winds in the north-south cross section (Fig. 3) are in rough agreement with this value, but those in the east-west cross section fall well below it. Although the assumption u (22 mb) = 0 may be inappropriate, there are other possible explanations for this discrepancy. The mean flow field determined by Mitchell *et al.* is characterized by a horizontal length $u\,(\partial u/\partial y)^{-1} = 2.5^{\circ}$ in longitude; hence the IRIS observations may not have fully resolved the horizontal gradients in temperature (c.f. Fig. 1). In addition, Mitchell *et al.* have argued that the effect of centripetal acceleration is not negligible at the eastern and western extremities of the GRS flow, because of the large radius of curvature there; they estimated Ro $\sim$ 0.36 locally. Inclusion of the centripetal term modifies (1) by the factor $f/(f + 2u/\mathcal{R})$, where $\mathcal{R}$ is the local radius of curvature. For anti-clockwise flow ($u > 0$) the factor is greater than unity for reasonable values of u, because $f < 0$. Since $\mathcal{R}$ scales roughly with distance from the center of the spot, the magnitude of this correction will be greatest at the inner portion of the vortex in Fig. 3a. Assuming u(500 mb) = 110 m s^{-1}, $\int_{22\ mb}^{500\ mb} \partial_p u\, dp$ nearly doubles in this region.

Tangential wind fields have not been presented at pressure levels above 22 mb, since temperatures in this region have larger errors. It is evident, however, that the warm core in the upper stratosphere (Fig. 2) implies, through Eq. (1), an increase in anticyclonic velocities with height above 22 mb. It follows from Fig. 2b that this buildup will be displaced southward by a few degrees from the vortex in Fig. 3.

Observations in the 5μm region enable one to probe levels well below 500 mb, because of the minimal gaseous absorption at that wavelength. Generally, cold temperatures at 5μm are thought to result from the presence of high altitude clouds, which block direct emission from the deeper, warmer layers of Jupiter's atmosphere (Terrile and Beebe, 1979); conversely, warm temperatures indicate relatively cloud-free regions. Observations at 5μm from the orthogonal scans are presented in Figure 4. The core of the GRS is cold at 5μm, but it is bounded by a region of enhanced emission. Other measurements, made during both Voyager encounters, have indicated that the region of enhanced 5μm emission forms a ring about the spot. This annular structure is least distinct east of the spot, where enhanced emission extends continuously over a broad range of longitudes. The observed 5μm structure agrees with ground-based observations reported by Terrile and Beebe (1979) and Terrile et al. (1979a,b). The highest temperature observed by IRIS at 5 μm near the GRS was 254 K (Fig. 4). With an average atmospheric temperature of 140 K at 500 mb and an adiabatic temperature lapse rate below that level (Hanel et al., 1979a), an emission level of 4 bars is implied. This temperature is actually a lower limit since the horizontal extent of the 254 K emissions may have been less than the projected IRIS field of view (5^{o} in latitude and longitude). However, observations of 5μm "hot spots" at higher spatial resolution made during the flybys suggest an upper limit of 260 K (Hanel, et al., 1979a).

For comparison, the brightness temperatures at 602 cm^{-1} which corrrespond to levels of the atmosphere near the tropopause, are also presented in Fig. 4. They are reasonably well correlated with the 5μm

emission. Bounding the cold temperatures over the GRS is a region in which the temperatures are approximately 1 K warmer than those further out. This warm ring is also evident in the cross-sections of atmospheric temperatures in Fig. 2. The implications of this structure will be discussed shortly.

The IRIS data imply that any infrared opaque clouds associated with the GRS lie at the 500 mb level or below. This conclusion follows from the absence of appreciable attenuation of the S(0) line of hydrogen and because the brightness temperatures at 226 cm^{-1} are consistently $\gtrsim$ 140 K. Hence appreciable absorption and emission from clouds can only occur at or below the 140 K level ($\sim$ 500 mb). Hanel et al. (1979b), from global infrared maps with lower spatial resolution ($\gtrsim 8^{\circ}$ in latitude and longitude), have found this to be the case over the entire planet.

Figure 5 presents radiometer and brightness temperature maps of the interior of the GRS. The maps are based on two observations per viewing site and the effective spatial resolution is 2° in longitude and 3° in latitude. Effects arising from varying emission (view) angle are small relative to the structure depicted in the maps. The albedos in the radiometer map are higher over the visible white feature in the northern portion of the GRS. This feature was remarked upon by Smith, et al., (1979a) and is suggestive of an overlying cloud. The high albedos are well correlated with the low temperatures in the 226 cm^{-1} brightness temperature map. In a clear atmosphere, this wavenumber would primarily sense levels near 800 mb (Hanel et al, 1979b), but more likely it is an indicator of clouds at higher altitudes. If we adopt T_{226} as a measure of cloudtop temperature and ignore the possible contribution from horizontal variations in NH_3 abundance (Hanel et al, 1979b), then we can estimate the relative height of the northern feature. With a lapse rate in temperature at p $\gtrsim$ 500 mb close to adiabatic (2 K km^{-1}), a temperature contrast of $\gtrsim$ 6 K implies that the $\tau_{226} = 1$ level of the northern white feature is $\gtrsim$ 3 km higher than the corresponding level over the rest of the GRS. Cloud opacities, on the other hand, should have minimal effect on the 602 cm^{-1} brightness temperature map (Fig. 5, top), which senses temperatures near the tropopause ($\gtrsim$ 150 mb). The horizontal structure is probably indicative of differential vertical motion, as discussed below and by Conrath et al. (1981).

Discussion

The Rossby number of the overall tangential flow of the GRS, inferred from visible cloud motions and integrated thermal winds, is small, implying that this flow is in geostrophic balance to a fair approximation. A high pressure core is therefore required at the levels of anticyclonic motion. The altitude of the visible clouds associated with the GRS is not precisely known; estimates range from 300 to 500 mb (Weidenschilling and Lewis, 1973; Gehrels, 1976; West and Tomasko, 1980). However, the absence of detectable infrared opaque clouds above 500 mb and the observed decrease in anticyclonic velocities above this level suggest that a high pressure core does exist at 500 mb. Unlike the terrestrial planets there is no solid surface on Jupiter (Stevenson and Salpeter, 1976); instead the interior is believed to be convective throughout (Hubbard, 1968). The convection is probably very efficient, and only negligibly small horizontal gradients in pressure and temperature can be maintained (Ingersoll, 1976a, Flasar and Gierasch, 1977, 1978). Therefore the presence of a high pressure core at 500 mb implies the existence of a warm core below this level but above that where thermally driven convection is efficient. It has been estimated that this latter region must be below the level at which water condensation occurs, i.e. $\sim$ 7 bars (Barcilon and Gierasch, 1970; Gierasch, 1976).

The cold tropopause can plausibly be explained in terms of vertical motion. The 5μm observations, presented earlier, suggest that the GRS itself is cloudy, but that there is an annular region about it devoid of high altitude clouds. If, by analogy with terrestrial tropical systems, cloudy areas can be associated with up-welling, adiabatic cooling, and condensation of a saturated gas (i.e., NH_3), then the 5μm data imply rising motion within the GRS and subsidence in a ring around it. The adiabatic cooling associated with the rising motion would give rise to a cold tropopause in the absence of local diabatic heating. By the same token, the adiabatic heating associated with the compensating subsidence should give rise to tropopause temperatures in the peripheral ring which are higher than the ambient value. Some evidence of this can be seen in the 602 cm^{-1} brightness temperatures in Fig. 4. Outside the cold core, there is a peripheral band with temperatures slightly higher than the background mean.

Hanel et al. (1979a) suggested that the structure in the stratosphere above the spot could be explained in terms of stationary quasi-geostrophic waves forced by the interaction of the geopotential high in the upper troposphere with an ambient mean flow. The decay of anticyclonic motions and temperature difference in the lower stratosphere would result from the decay of shorter-wavelength components, which cannot propagate vertically in the stratosphere (Charney and Drazin, 1961). The penetration height, f L/N, where L is the horizontal scale of the GRS and N the Brunt-Vaisalla frequency, is about two scale heights, in agreement with the data (Figs. 2 and 3). The structure in the upper stratosphere ($p < 10$ mb) would be a manifestation of the longer wavelength components, which can propagate vertically provided the ambient flow in the stratosphere is eastward. This hypothesis is investigated quantitatively in the Appendix by means of a simple model. The difficulty with this interpretation is that the theoretical model predicts that vertically propagating wave disturbances should only appear downstream from the GRS, i.e., east of it, whereas Fig. 2a suggests that the thermal structure in the upper stratosphere is symmetric about the central longitude of the spot. The discrepancy might be explained by the simplicity of the model: linearized wave propagation in a background zonal flow which is uniform. The anticyclonic velocities of the GRS are probably not small compared to the ambient zonal flow. Nevertheless we feel that the qualitative disagreement suggests that the structure above the GRS in the stratosphere is not a direct manifestation of the thermal field associated with vertically propagating waves.

Previous theoretical models of the dynamics of the GRS have fallen naturally into two classes: those which treat the spot as a free solution of the inviscid potential vorticity equation, and those which are mainly concerned with the energy drive of the GRS. Ingersoll (1973) was able to construct steady solutions of the barotropic vorticity equation to obtain circulation patterns which resemble those of the GRS and the neighboring currents. Maxworthy and Redekopp (1976) (see also Redekopp, 1977; Maxworthy et al, 1978) have considered a special class of nonlinear neutral solutions of the baroclinic potential vorticity equation, solitons, in which the tendency of nonlinear advection to steepen the waves is balanced by

dispersion. They argued that the GRS is localized near the tropopause and is not a deep-seated circulation. Although their model does predict cooler temperatures at the tropopause, it does not naturally explain the peripheral warm ring observed at that level. Moreover, the observed decrease in anticyclonic vorticity above 500 mb, the necessity for a warm core below that level, and the subsidence down to at least 4 bars implied by the 5 μm data all suggest that the GRS circulation does extend into the deep atmosphere.

The manner in which these free solutions are maintained against frictional and radiative dissipation is not treated in the models. Maxworthy and Redekopp (1976; see also Redekopp, 1977) hypothesized that waves which are slightly unstable barotropically can extract energy from the horizontal shear of the background zonal flow. However, the manner in which the precise balance between unstable growth and dissipation is preserved has not been delineated. Perhaps the chief value of the free solution models in their present form is that they are capable of reproducing the observed horizontal flow, suggesting that the required forcing in the presence of dissipation need not be very special.

The energy source driving the GRS and producing the warm core beneath the visible cloudtop is not known, but the inferred upward motion within the spot suggests that it may be associated with the latent heat release of condensing water vapor. Several authors (Barcilon and Gierasch, 1970; Gierasch, 1976; Ingersoll, 1976b) have emphasized the role that latent heat release may have in maintaining the zone - belt circulation. Kuiper (1972) drew a close analogy between the GRS and tropical cyclones (hurricanes) on Earth for which the heating from water vapor condensation plays a central role. Ingersoll (1976b) has noted that the GRS is dynamically similar to a hurricane since both (excluding the hurricane's eye) have warm cores of rising motion, but stressed that the details of their low-level moisture convergence probably differ. This is because a tropical cyclone is bounded below by a well-defined horizontal surface -- the ocean -- along which pressure gradients can be maintained, and therefore convergence is associated with a low pressure center. On the other hand, the GRS is bounded below by an adiabatic fluid, in which horizontal pressure gradients

are negligible. Thus low-level convergence may result primarily from the balance between the frictional stress generated by the overlying anticyclonic vortex and the Coriolis torque on the radial velocity, much as it is in the wind-driven upper layers of the terrestrial oceans. Ingersoll also suggested that the existence of a low pressure core at the surface explains why hurricanes are strongly cyclonic through most of the troposphere and only weakly anti-cyclonic at the tropopause level ($\sim$ 100 mb).

A simplified model which serves as a useful vehicle for comparing the dynamics of tropical cyclones and the GRS is that of a frictionally controlled axisymmetric vortex. Ogura (1964) has considered this model in the limit where the Rossby number, Ro, is of order unity or greater and applied it to hurricanes. The case in which Ro << 1 is outlined in the appendix of the companion paper by Conrath et al. (1981). Table 1 compares the observed properties of tropical cyclones, taken from the composited data of Frank (1977a) and Shea and Gray (1973), with those of the GRS. Comparisons are made of the tropopause and the lower troposphere. In Table 1 tangential velocities are defined to be positive if they are cyclonic.

Hurricane anticyclonic velocities are strongest near the tropopause. At this level the tangential velocities increase more or less linearly with radius to $\sim$ 1300 km from the center of the storm; they do not have the annular structure implied by Fig. 3 for the GRS. Although the hurricane anticyclonic velocities are weaker than those of the GRS, the Rossby number is greater, Ro = O(1), and the tangential velocities are not in geostrophic balance: the contribution of the nonlinear centripetal acceleration to the radial momentum equation is significant. The larger value of Ro for the terrestrial storm is a consequence of the smaller Coriolis frequency and horizontal dimension.

Like the GRS, a hurricane exhibits a cold core, with maximum thermal contrast occurring near the tropopause level. The cold temperatures are believed to result from cumulonimbus overshooting (Frank, 1977a,b). The Burger number, ε, and the Richardson number, Ri, are measures of the mean vertical stratification ($\bar{N}$ is the horizontally averaged Brunt-Vaisala

frequency). For an axisymmetric, frictionally controlled vortex, these nondimensional quantities arise in the dynamical scaling of the thermodynamic heat equation (Conrath et al, 1981; Ogura, 1964). When $Ro \leq 1$, $\epsilon\ Ro^{-1}$ measures the magnitude of the effect of vertical motions acting on the mean, or basic state, temperature field relative to the nonlinear advective terms in the heat equation; Ri measures the corresponding ratio when $Ro \geq 1$. According to Table 1, $Ro < 1$ and $\epsilon\ Ro^{-1} >> 1$ for both the GRS and the hurricane at the tropopause; the adiabatic cooling associated with rising motion, therefore, should dominate and produce the cold tropopauses which are observed.

Although the circulation in the lower troposphere of a tropical cyclone typically extends out to $\sim 10^3$ km, the largest tangential velocities and horizontal gradients in temperature occur over the inner 10^2 km. The maximum cyclonic tangential velocities occur near 850 mb and are of the same order as those observed for the GRS. The horizontal scale of the hurricane in this part of the atmosphere is so small that, above the frictional surface boundary layer, the tangential flow is cyclostrophic: the centripetal acceleration nearly balances the radial pressure gradient. The estimate, $Ri \sim 1$, implies that horizontal and vertical advection of heat are comparable; the lowest order balance in the heat equation is therefore nonlinear.

The parameters for the GRS below the visible cloud deck are highly uncertain. The horizontal scale has been assumed to be similar to that observed at the cloud top level. Uncertainties in this scale affect the estimates of Ro and ϵ. The GRS vertical scale has been chosen on the assumption that the water clouds are dynamically important. The horizontal temperature contrast, 6 K, is that value which, upon integrating the thermal wind relation, (1), from the base of the water clouds, ~ 7 bars (Gierasch, 1976), produces a 100 m s^{-1} anticyclonic wind at the 500 mb level. This is three times the thermal contrast which is estimated, using the solar abundance of water ($q \sim 8 \times 10^{-3}$ g H_2O/g atmosphere) from the relation

$$C_p\ dT \sim T\ d\left(\frac{qh}{T}\right) \qquad (2)$$

(cf. Holton, 1972; C_p is the specific heat at constant pressure, T is temperature, and h the latent heat of condensation) and the assumption of saturated updrafts and dry downdrafts (Gierasch, 1976; Ingersoll, 1976b). It is open to question just how meaningful this last assumption is, since moist convection on Earth exhibits a much more complex behavior. The estimates of ε and Ro in Table 1 for the GRS do suggest a flow in the lower troposphere similar to that inferred for the tropopause: that of a frictionally controlled vortex in which geostrophic balance and adiabatic heating or cooling associated with vertical motions dominate. As discussed in detail by Conrath et al. (1981), such a system is linear relative to the basic state fields.

Although a tropical cyclone, viewed as a frictionally controlled axisymmetric vortex, is highly nonlinear, the GRS, excluding the nonlinearities of the latent heat release process, may allow a linear description of its large-scale motions (Conrath et al., 1981), and in this sense represent a simpler dynamical system. The parameterization of moist convection in Jupiter's atmosphere, however, is not known. It is not clear how useful a guide terrestrial experience will be, since the lower boundaries on Earth and Jupiter are so different. Nonetheless, questions such as this must be addressed if the viability of the latent heat hypothesis for the GRS is to be realistically assessed.

Summary and Conclusions

Consistent with ground-based measurements, low 5 μm brightness temperatures are observed by IRIS over the GRS, indicating the presence of relatively high-altitude clouds; high temperatures are detected in a peripheral cloud-free ring about the spot, with emission from levels $\geq$ 4 bars. The atmospheric temperatures near the tropopause exhibit a similar structure: there is a well-defined cold core surrounded by a peripheral band in which temperatures appear slightly warmer than the background mean. These data are consistent with a local circulation in which there is rising motion within the spot and subsidence in an annular region about it. The adiabatic cooling and heating associated with this vertical motion are responsible for the observed thermal structure at the tropopause.

The cold temperatures above the spot imply a despinning of anticyclonic motion with height above 500 mb into the lower stratosphere. This, coupled with the fact that infrared opaque clouds are not detected above 500 mb, implies the presence of a high pressure core over the spot at this level. This necessitates the existence of a warm core and an attendant source of heating at deeper levels of the atmosphere, which is consistent with the deep circulation suggested by the 5μm data.

The energy source which produces the warm core below 500 mb and the vertical motions described above is not known, but latent heat release associated with water vapor condensation is a viable candidate. The dynamical scalings based on an axisymmetric, frictionally controlled vortex, which appear capable of explaining the gross structure of both the GRS and tropical cyclones, suggest that, aside from the nonlinearities inherent in the latent heat release process, the large-scale dynamics of the GRS are linear, whereas those of a tropical cyclone are markedly nonlinear. In addition, as previously noted by Ingersoll (1976b), the lower boundaries are quite different for the two systems. To achieve further progress in modeling the GRS dynamics, based on latent heat exchange, requires a fundamental study of the parameterization of moist convection in a deep atmosphere.

Finally, the IRIS data indicate temperatures in the upper stratosphere over the GRS which are warmer than those in the surrounding region. An earlier suggestion by Hanel et. al. (1979a), that the temperatures at these altitudes are a manifestation of vertically propagating Rossby waves, appears to be inconsistent with the observed spatially resolved thermal structure.

Acknowledgements

We thank L. Horn (JPL) for helping to verify the locations of the IRIS field of view during the GRS observing sequence, J. Hornstein (Computer Sciences Corporation) for his assistance in the programming and execution of the temperature retrieval algorithm, and R. A. Hanel (GSFC) for a critical reading of the manuscript.

APPENDIX. Stratospheric Waves Driven by Geopotential Forcing at the Tropopause

Hanel et al. (1979a) suggested that the thermal structure in the stratosphere above the GRS could be understood in terms of vertically propagating waves, forced by the interaction of the geopotential high at the tropopause with the ambient mean flow. For scales of interest and for stratospheric winds of a few tens of meters per second, the frequencies excited within the stratosphere are less than the Coriolis frequency. Inertia-gravity waves are therefore not excited and the dynamics is quasi-geostrophic. The simplest model is one in which the ambient stratospheric flow is uniform, the forcing is stationary, motions are adiabatic and inviscid, and the β-approximation is adopted. The resulting linearized dynamics is well understood (Charney and Drazin, 1961; Holton, 1975). The linear variables can all be expressed in terms of the perturbation geopotential ϕ, and a single Fourier component,

$$\phi(x,y,z) = \phi_{k\ell}\, e^{z/2H}\, e^{i(kx + \ell y + nz)}, \qquad (A.1)$$

yields the dispersion relation,

$$n^2H^2 = \frac{\beta \mathcal{L}^2}{\bar{u}} - \frac{1}{4}\mathcal{L}^2(k^2 + \ell^2) \qquad (A.2)$$

Here, x, y, and z dencte eastward, northward, and vertical (log-pressure) coordinates, and k, ℓ, and n are the corresponding wavenumbers; $\beta = df/dy$, $\bar{u}$ is the mean stratospheric wind, H is the scale height, and $\mathcal{L}$ is the Rossby deformation radius,

$$\mathcal{L} = \frac{N}{f} H \qquad (A.3)$$

(Detailed definitions of most of the symbols used in this section can be found in the appendix of the companion paper by Conrath, et al., 1981).

When $n^2 > 0$, the requirement that energy propagate upward requires $n/k < 0$; when $n^2 < 0$, boundedness as $z \to \infty$ requires $Im(n) > 0$. Calculations have been made with an imposed geopotential disturbance at the tropopause (z=0) of the form,

$$\phi(x,y,z=0) = \phi_o e^{-(x^2 + y^2)/a^2} \qquad (A.4)$$

The computation is straightforward. The Fourier transform of (A.4) gives $\phi_{k\ell}$ and the inverse transform of (A.1) gives the predicted $\phi(x,y,z)$. Other quantities of interest can then be evaluated from the equations of motion (see, for example, Holton, 1975).

From (A.2), vertical propagation ($n^2 > 0$) is only possible for eastward mean flows ($\bar{u} > 0$) which are less than the critical value,

$$\bar{u}_c = 4\beta \mathcal{L}^2 \qquad (A.5)$$

For a mean statospheric lapse rate, $\partial T/\partial z = 1$ K km^{-1}, $\mathcal{L} \lesssim 4000$ km and $\bar{u}_c \lesssim 290$ m s^{-1} at a latitude of 23°, which most likely is far in excess of the magnitudes of the mean winds in the stratosphere of Jupiter. A forced disturbance of the form (A.4) will excite modes with wavenumbers $(k^2 + \ell^2)^{1/2} \leq a^{-1}$. Since longer wavelength modes are favored for vertical propagation (A.2), it follows that larger-scale forcing ($\beta a^2/\bar{u} \gtrsim 1$) produces vertically propagating waves more efficiently. Figure 6 illustrates the range of behavior which can be produced by different scales of forcing. Three cases are presented, representing weak, marginal, and strong vertical propagation. The thermal structure in the latter two cases exhibits a downstream (eastward) tilt, which is caused by the β term. The corresponding north-south cross sections are symmetric about the central latitude of the forcing.

A comparison with the observed thermal structure over the GRS is instructive. In contrast to the model, the stratospheric temperature fields depicted in Figure 2 are not symmetric with respect to the central latitude

($23^{\circ}S$), whereas they are roughly symmetric about the c.
($77^{\circ}W$). The observed north-south asymmetry might result from the spatial variation of $\bar{u}$. Indeed, the zonally averaged flow observed at the visible cloud tops exhibits a marked meridional shear, progressing from westward to eastward velocities as one moves southward over the range of latitudes occupied by the spot (Ingersoll et al., 1979; Smith et al., 1979b). It is not unreasonable to suppose that the sense of the zonal flow persists through at least part of the stratosphere. On the other hand, the eastward tilt of the thermal structure predicted by the model appears to be more fundamental. The analytic, β-plane study by Simmons (1974; see the discussion in Holton, 1975) suggests that such a tilt remains when $\bar{u}$ is nonuniform; the effect of lateral shear and uniform vertical shear on the dispersion equation is only to modify the effective β in (A.2). Perhaps the basic failing of the model is that it is linear. The criterion for linearity to be valid is that the perturbation velocities be small relative to $\bar{u}$. In contrast, the visible cloud motions (Smith et al, 1979a) indicate that the tangential velocities of the GRS are comparable to the mean zonal velocities, and, indeed, the zonal flow is substantially modified in the vicinity of the spot. According to Figure 3, the GRS vortex remains well defined above the tropopause.

References

Barcilon, A. and P. Gierasch, A moist, Hadley cell model for Jupiter's cloud bands, J. Atmos. Sci., 27, 550-560, 1970.

Charney, J.R. and P.G. Drazin, Propagation of planetary-scale disturbances from the lower into the upper atmosphere, J. Geophys. Res., 66, 83-109, 1961.

Conrath, B.J., F.M. Flasar, J.A. Pirraglia, P. Gierasch, and G.E. Hunt, Thermal structure and dynamics of the Jovian atmosphere. II. Visible Cloud Features, J. Geophys Res., this issue, 1981.

Conrath, B.J., and D. Gautier, Thermal structure of Jupiter's atmosphere obtained by inversion of Voyager 1 infrared measurements, in Interpretation of Remotely Sensed Data, ed. by A. Deepak, Academic Press, New York, 1980.

Flasar, F.M., and P.J. Gierasch, Eddy diffusivities in Jupiter, in Proceeding: Symposium on Planetary Atmospheres, ed. A.V. Jones, Royal Society of Canada, pp. 85-87, 1977.

Flasar, F.M. and P.J. Gierasch, Turbulent convection within rapidly rotating superadiabatic fluids with horizontal temperature gradients, Geophys. Astrophys. Fluid Dynamics, 10, 175-212, 1978.

Frank, W.M., The structure energetics of the tropical cyclone. 1. Storm structure, Mon. Weather Rev., 105, 1119-1145, 1977a.

Frank, W.M., Convective fluxes in tropical cyclones, J. Atmos. Sci., 34, 1554-1568, 1977b.

Gehrels, T., The results of the imaging photopolarimeter on Pioneers 10 and 11, in Jupiter: Studies of the Interior, Atmosphere, Magnetosphere, and Satellites, ed. T. Gehrels, U. Ariz. Press, pp. 531-563, 1976.

Gierasch, P.J., Jovian meteorology: Large-scale moist convection, Icarus, 29, 445-454, 1976.

Hanel, R., B. Conrath, M. Flasar, V. Kunde, P. Lowman, W. Maguire, J. Pearl, J. Pirraglia, R. Samuelson, D. Gautier, P. Gierasch, S. Kumar and C. Ponnamperuma, Infrared observations of the Jovian system from Voyager 1, Science, 204, 972-976, 1979a.

Hanel, R., B. Conrath, M. Flasar, L. Herath, V. Kunde, P. Lowman, W. Maguire, J. Pearl, J. Pirraglia, R. Samuelson, D. Gautier, P. Gierasch, L. Horn, S. Kumar and C. Ponnamperuma, Infrared observations of the Jovian system from Voyager 2, Science, 206, 952-956, 1979b.

Holton, J.R. An Introduction to Dynamic Meteorology, Academic Press, New York, 1972.

Holton, J.R., The Dynamical Meteorology of the Stratosphere and Mesosphere, Amer. Met. Soc., Boston, 1975.

Hubbard, W.B., Thermal structure of Jupiter, Astrophys. J., 152, 745-754, 1968.

Ingersoll, A.P., Jupiter's Great Red Spot: A free atmospheric vortex? Science 182, 1346-1348, 1973.

Ingersoll, A.P., Pioneer 10 and 11 observations and the dynamics of Jupiter's atmosphere, Icarus, 29, 245-253, 1976a.

Ingersoll, A.P., The atmosphere of Jupiter, Space Sci. Rev., 18, 603-639, 1976b.

Ingersoll, A.P., R.F. Beebe. S.A. Collins, G.E. Hunt, J. L. Mitchell, P. Muller, B.A. Smith, and R.J. Terrile, Zonal velocity and texture in the Jovian atmosphere from Voyger images, Nature, 280, 773-775, 1979.

Kuiper, G.P., Lunar and Planetary Laboratory studies of Jupiter - II, Sky and Telescope, 43, 75-81, 1972.

Maxworthy, T. and L.G. Redekopp, A solitary wave theory of the Great Red Spot and other observed features in the Jovian atmosphere, Icarus, 29, 261-271, 1976.

Maxworthy, T., L.G. Redekopp, and P.D. Weidman, On the production and interaction of planetary solitary waves: Applications to the Jovian atmosphere, Icarus, 33, 388-409, 1978.

Mitchell, J.L., R.F. Beebe, A.P. Ingersoll, and G.W. Garneau, Flow fields within Jupiter's Great Red Spot and white oval BC, J. Geophys. Res., this issue, 1981.

Ogura, Y., Frictionally controllled, thermally driven circulations in a ciruclar vortex with application to tropical cyclones, J. Atmos. Sci., 21, 610-621, 1964.

Orton, G.S., The thermal structure of Jupiter. I. Implications of Pioneer 10 infrared radiometer data, Icarus, 26, 125-141, 1975.

Peek, B.M., The Planet Jupiter, Faber and Faber, London, 1958.

Redekopp, L.G., On the theory of solitary Rossby waves, J. Fluid Mech., 82, 725-745, 1977.

Shea, D.J., and W.M. Gray, The hurricane's inner core region. I. Symmetric and asymmetric structure, J. Atmos. Sci, 30, 1544-1564, 1973.

Simmons, A.J., Planetary scale disturbances in the polar winter stratosphere, Quart. J. Roy. Meteor. Soc., 100, 76-108, 1974.

Smith, B.A., L.A. Soderblom, T.V. Johnson, A.P. Ingersoll, S.A. Collins, E.M. Shoemaker, G.E. Hunt, H. Masursky, M.H. Carr, M.E. Davies, A.F. Cook II, J. Boyce, G.E. Danielson, T. Owen, C. Sagan, R.F. Beebe, J. Veverka, R.G. Strom, J.F. McCauley, D. Morrison, G.A. Briggs, and V.E. Suomi, The Jupiter system through the eyes of Voyager 1, Science, 204, 951-972, 1979a.

Smith, B.A., R. Beebe, J. Boyce, G. Briggs, M. Carr, S.A. Collins, A.F. Cooke II, G.E. Danielson, M.E. Davies, G.E. Hunt, A. Ingersoll, T.V. Johnson, H. Masursky, J. McCauley, D. Morrison, T. Owen, C. Sagan, E.M. Shoemaker, R. Strom, V.E. Suomi, and J. Veverka, The Galilean satellites and Jupiter: Voyager 2 imaging science results, Science, 206, 927-950, 1979b.

Stevenson, D.J. and E.E. Salpeter, Interior models of Jupiter, in Jupiter: Studies of the Interior, Atmosphere, Magnetosphere, and Satellites, ed. T. Gehrels, Univ. Az. press, pp 85-112, 1976.

Terrile, R.J. and R.F. Beebe, Summary of historical data: Interpretation of the Pioneer and Voyager cloud configurations in a time-dependent framework, Science, 204, 948-950, 1979.

Terrile, R.J., R.W. Capps, D.E. Backman, E.E. Becklin, D.P. Cruikshank, C.A. Beichman, R.H. Brown and J.A. Westphal, Infrared images of Jupiter at 5-micrometer wavelengths during the Voyager 1 encounter, Science, 204, 1007-1008, 1979a.

Terrile, R.J., R.W. Capps, E.E. Becklin, and D.P. Cruikshank, Jupiter cloud distribution between the Voyager 1 and 2 encounters: Results from 5-micrometer Imaging, Science, 206, 995-996, 1979b.

Weidenschilling, S.J., and J.S. Lewis, Atmospheric and cloud structures of the Jovian planets, Icarus, 20, 465-476, 1973.

West, R.A., and M.G. Tomasko, Spatially resolved methane band photometry of Jupiter. III. Cloud vertical structures for several axisymmetric bands and the Great Red Spot, Icarus, 41, 278-292, 1980.

Table 1

	Tropical Cyclone	GRS
Tropopause level (mb)	100	150
$T_{center} - T_{environment}$ (K)	-2	-10
Horizontal dimension: L (km)	10^3	10^4
Vertical Scale: D (km)	6	25
Tangential velocity: U ($m\ s^{-1}$)	-10	-50
Rossby Number: $Ro = U\ (fL)^{-1}$	0.5	10^{-1}
Burger Number: $\epsilon = \left(\frac{N}{f}\ \frac{D}{L}\right)^2$	7	1
Richardson Number: $Ri = \epsilon\ Ro^{-2}$	30	10^2
Lower troposphere (mb)	980-200	>500
$T_{center}-T_{environment}$ (K) (max.)	15	6
Horizontal dimension: L(km)	10^2	10^4(?)
Vertical Scale: D(km)	8	100
Tangential Velocity: U($m\ s^{-1}$)	90	-100
Rossby Number: Ro	20	10^{-1}
Burger Number: ϵ	300	≤ 1
Richardson Number: Ri	1	$\leq 10^2$

Figure Captions

Figure 1: Inner portion of the GRS "cross" sequence. The IRIS fields of view are superposed on narrow angle images taken during the sequence.

Figure 2: (a) East-west vertical cross section of temperature fields over the GRS. (b) North-south vertical cross section of temperature fields over the GRS. The temperatures are deviations (K) from an average temperature profile.

Figure 3: (a) East-west vertical cross section of thermal wind fields over the GRS. Positive numbers indicate northward velocities. (b) North-south vertical cross section of thermal winds over the GRS. Positive values indicate eastward velocities. In (a) and (b) the velocities at 22 mb have been specified to be zero.

Figure 4: Brightness temperatures at 602 cm^{-1} and 5μm, along the major and minor axes of the GRS. The temperatures are actually averages over 581-619 cm^{-1} and 2001-2050 cm^{-1}, respectively. The signal when $T_{5\mu m} < 200$ K is within the noise level of the instrument.

Figure 5: Interior of the GRS. Bottom: IRIS radiometer map of reflected solar radiation (500-2500 cm^{-1}) in relative units. Middle: Brightness temperature map at 226 cm^{-1}. In a clear atmosphere this wavenumber would sense a range of pressure weighted at 800 mb, but in all probability it is sensing clouds at $p > 500$ mb. Top: Brightness temperature map at 602 cm^{-1} (581-619 cm^{-1} average), corresponding to a pressure level of approximately 150 mb. The maps are superposed on a Voyager 1 image obtained during the mapping sequence.

Figure 6: A model of the stratospheric perturbation temperatures created by a circular Gaussian disturbance at the tropopause. For all three panels $\beta L^2/\bar{u} = 3.0$, which corresponds to $\bar{u} = 25$ m s^{-1} at 23°

latitude and L = 4000 km. The smallest spot size (top) results in weak propagation. Middle: An intermediate case, in which there is marginal propagation. Bottom: A spot the size of the GRS's minor axis exhibits strong propagation, and the strength of the propagation has resulted in an asymmetric temperature field in which the cold region over the spot center has disappeared. The magnitude of the tropospheric forcing has been specified in each of the three cases to emphasize the stratospheric thermal structure.

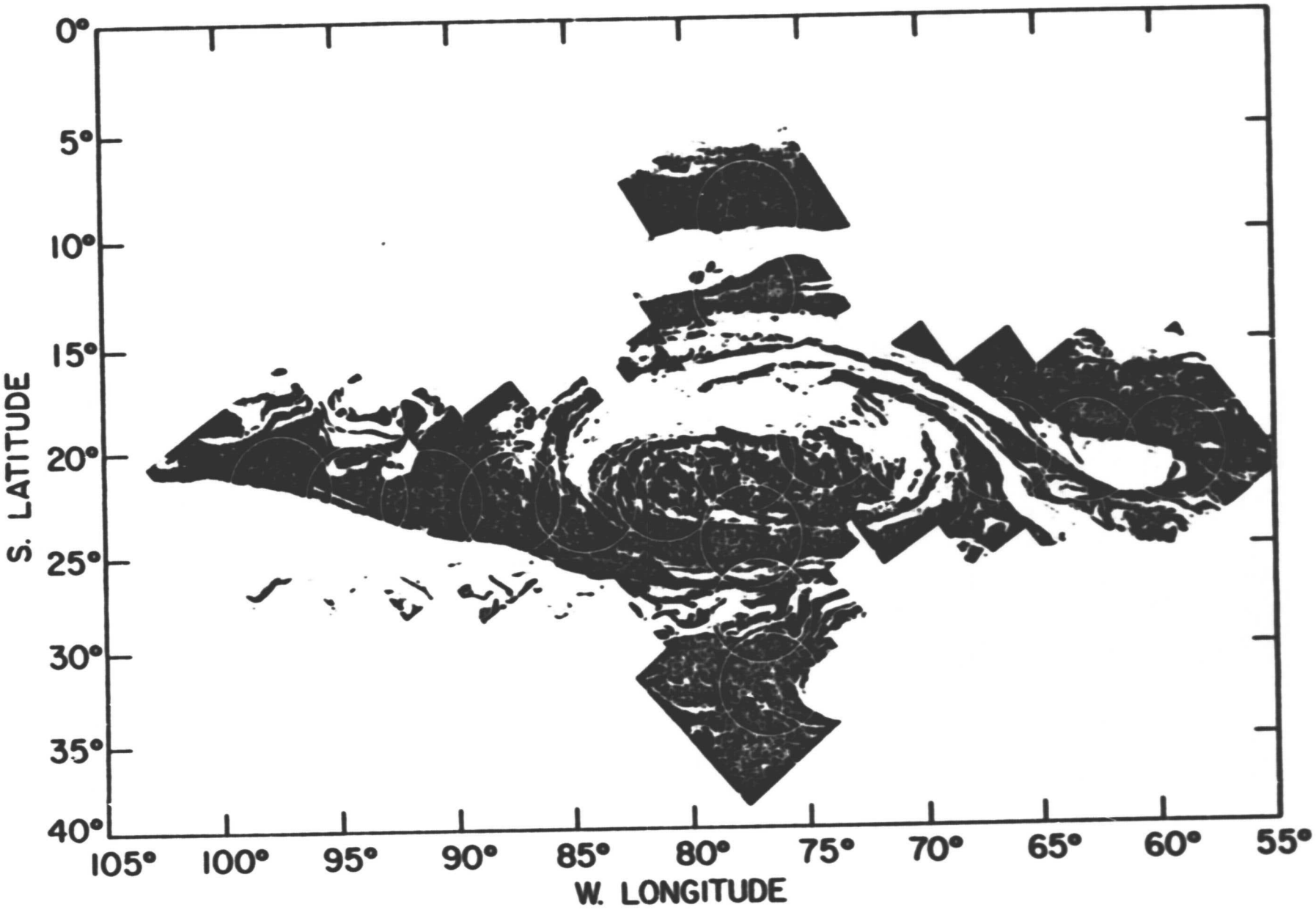

Figure 1

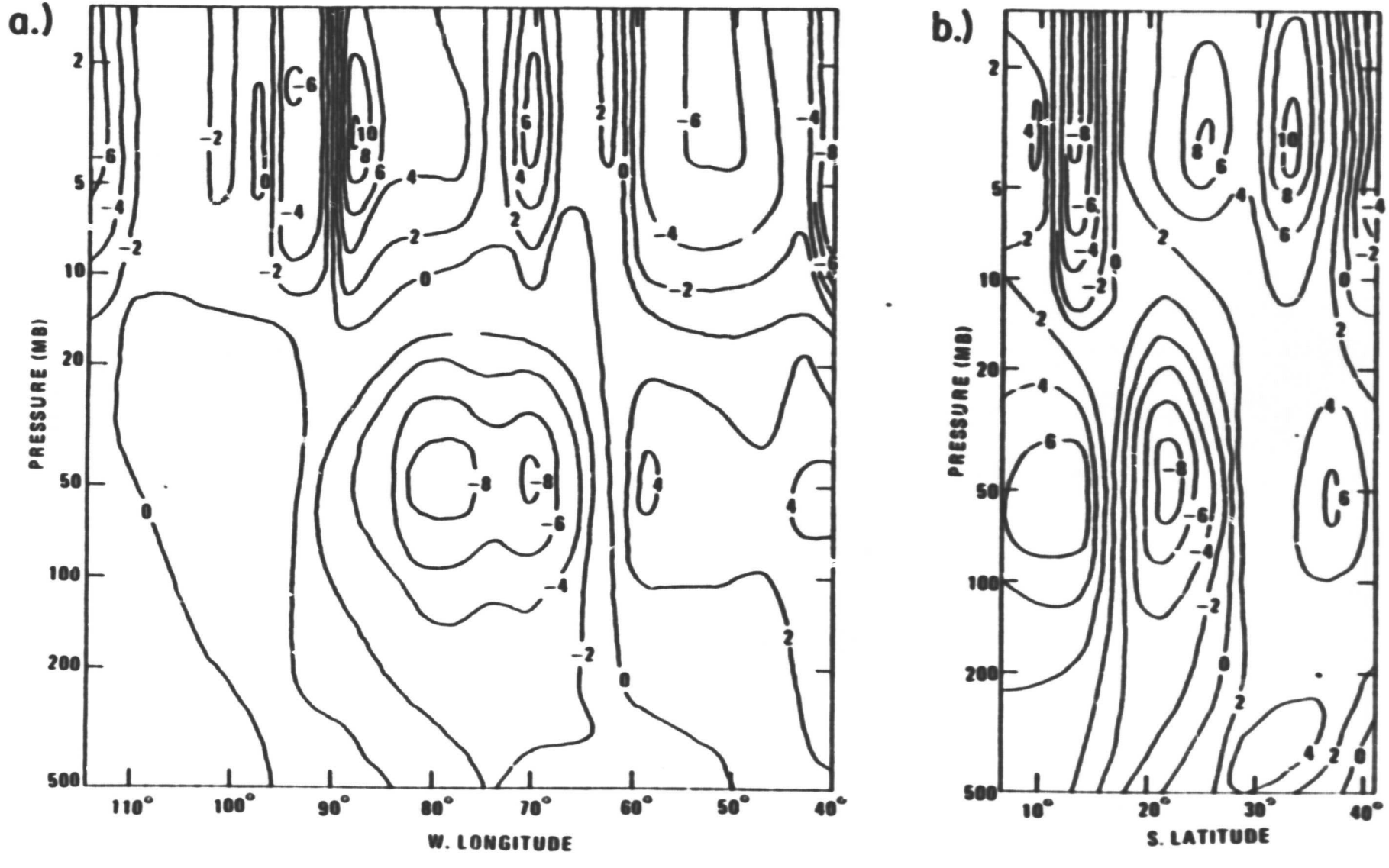
a.)
PRESSURE (MB)
2
5
10
20
50
100
200
500
110°
100°
90°
80°
70°
60°
50°
40°
W. LONGITUDE
b.)
PRESSURE (MB)
2
5
10
20
50
100
200
500
10°
20°
30°
40°
S. LATITUDE

Figure 2

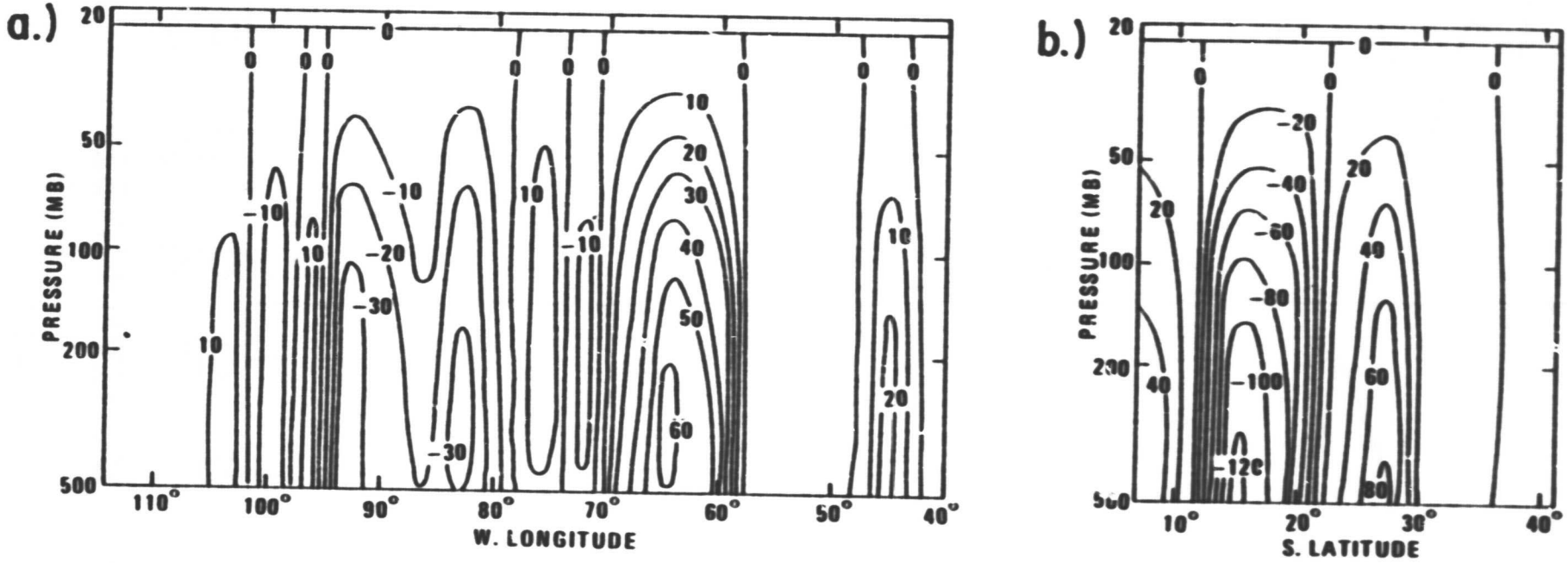

Figure 3

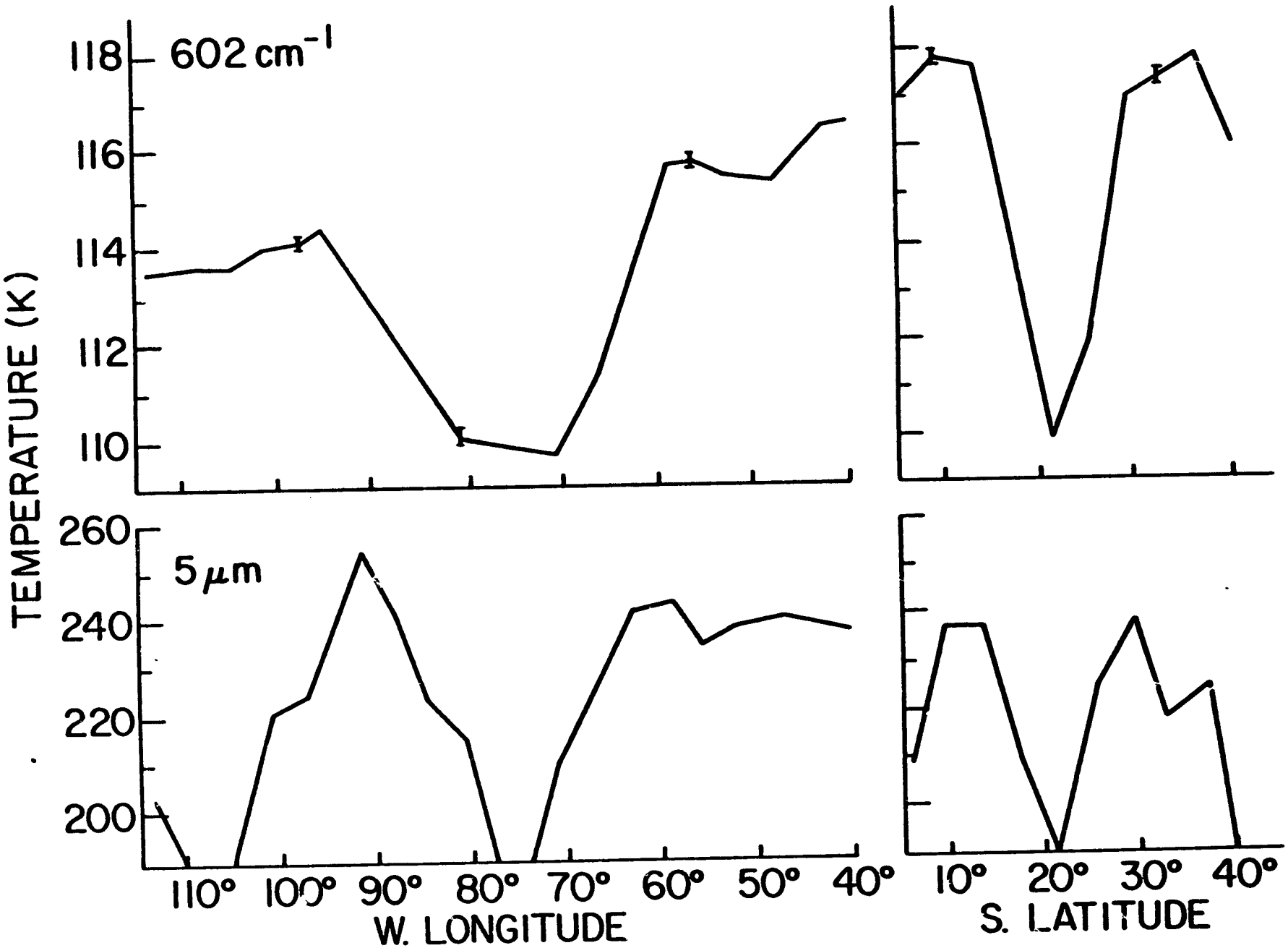
602 cm⁻¹
118
116
114
112
110
5 μm
260
240
220
200
TEMPERATURE (K)
110° 100° 90° 80° 70° 60° 50° 40°
W. LONGITUDE
10° 20° 30° 40°
S. LATITUDE

Figure 4

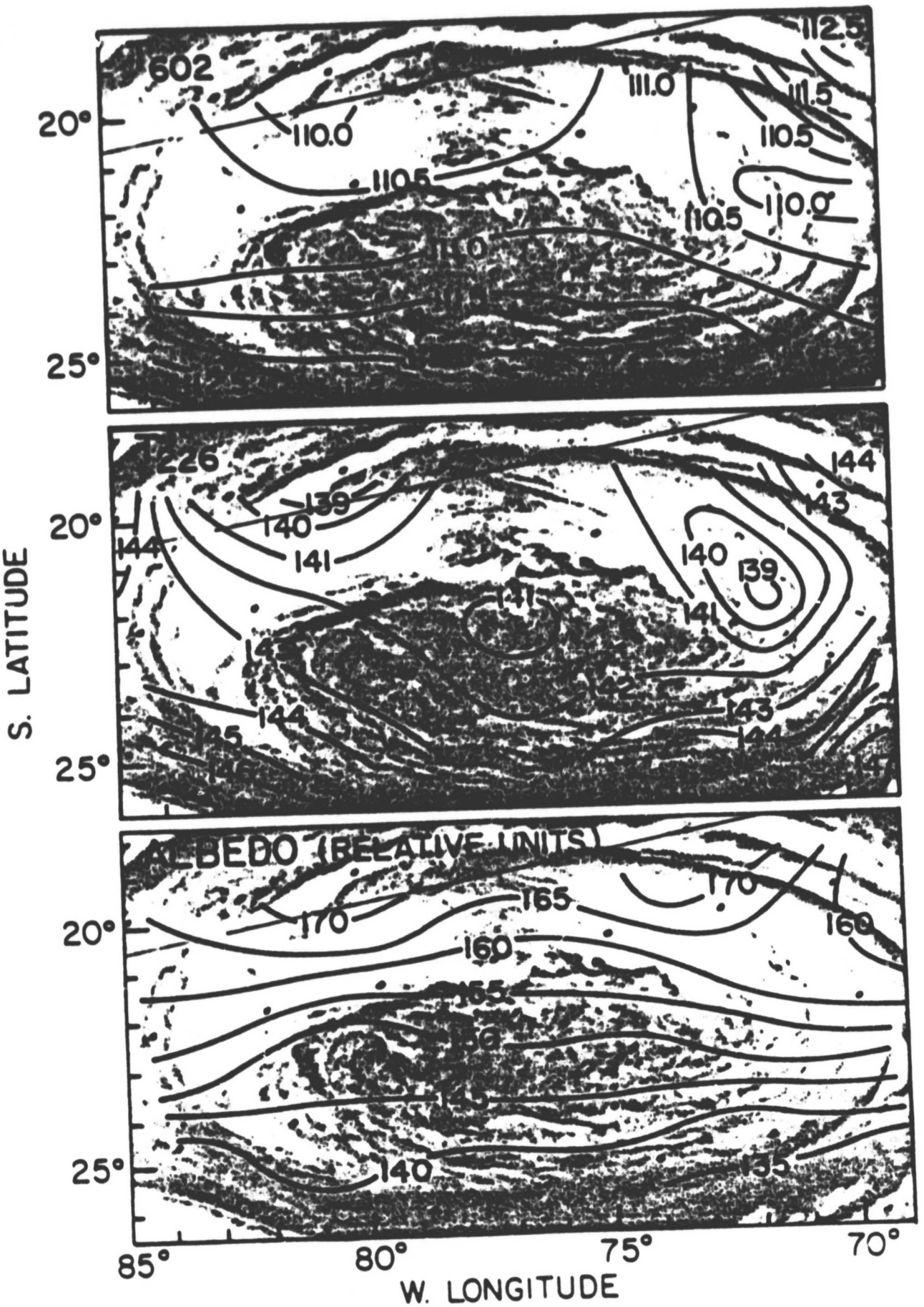

Figure 5

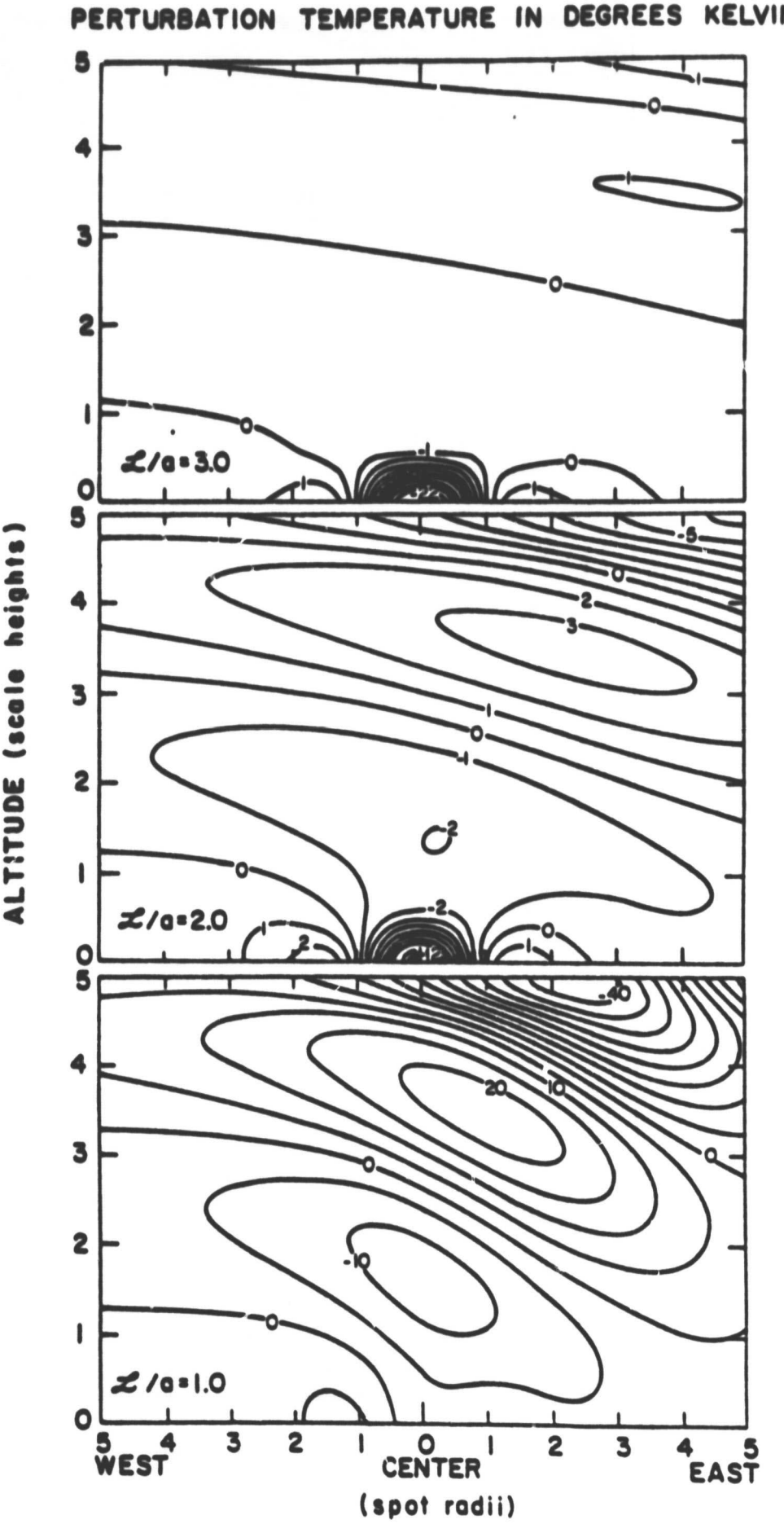
PERTURBATION TEMPERATURE IN DEGREES KELVIN
ALTITUDE (scale heights)
ℒ/a=3.0
ℒ/a=2.0
ℒ/a=1.0
WEST
CENTER
EAST
(spot radii)

Figure 6